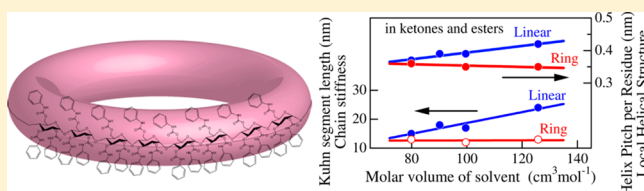


Local Conformation and Intermolecular Interaction of Rigid Ring Polymers Are Not Always the Same as the Linear Analogue: Cyclic Amylose Tris(phenylcarbamate) in Θ Solvents

Natsuki Asano,[†] Shinichi Kitamura,[‡] and Ken Terao^{*,†}[†]Department of Macromolecular Science, Graduate School of Science, Osaka University, 1-1 Machikaneyama-cho, Toyonaka, Osaka 560-0043, Japan[‡]Graduate School of Life and Environmental Sciences, Osaka Prefecture University, Gakuen-cho, Nakaku, Sakai, 599-8531, Japan

S Supporting Information

ABSTRACT: Small-angle X-ray scattering and static and dynamic light scattering measurements were made for cyclic amylose tris(phenylcarbamate) (cATPC) of which weight-average molar mass M_w ranges from 1.3×10^4 to 1.5×10^5 to determine their z -average mean square radius of gyration $\langle S^2 \rangle_z$, particle scattering function $P(q)$, hydrodynamic radius R_H , and second virial coefficient A_2 in methyl acetate (MEA), ethyl acetate (EA), and 4-methyl-2-pentanone (MIBK). The obtained $\langle S^2 \rangle_z$, $P(q)$, and R_H data were analyzed in terms of the wormlike ring to estimate the helix pitch per residue h and the Kuhn segment length λ^{-1} (the stiffness parameter, twice the persistence length). Both h and λ^{-1} for cATPC in MEA, EA, and MIBK are smaller than those for linear amylose tris(phenylcarbamate) (ATPC) in the corresponding solvent and the discrepancy becomes more significant with increasing the molar volume of the solvent. This indicates that not every rigid ring has the same local helical structure and chain stiffness as that for the linear polymer in the M_w range investigated while infinitely long ring chains should have the same local conformation. This conformational difference also affects A_2 . In actuality, negative A_2 was observed for cATPC in MIBK at the Θ temperature of linear ATPC whereas intermolecular topological interaction of ring polymers increases A_2 .

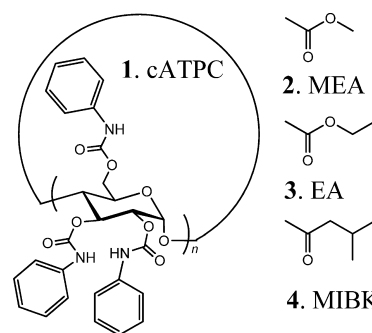


INTRODUCTION

How are ring polymer chains different from the corresponding linear chains? When the chain is flexible enough and long enough, its local conformation should be essentially the same as those for the linear polymer. But, if the chain has sufficient high stiffness with a finite chain length, the local curvature of rigid rings may influence the local conformation and then the intermolecular interactions. Even though much work has been done for flexible ring polymers in dilute solution, that is, poly(dimethylsiloxane),^{1,2} polystyrene,^{3–10} and amylose,^{11–13} few rigid ring polymers have been reported except for some macrocyclic brushes^{14–16} and cyclic DNA. Thus, quantitative discussion for the conformational difference between non-flexible linear and ring polymers has not been reported yet except for superhelix formation of double helical cyclic DNA.

Recently, taking high chain stiffness of amylose carbamates^{17,18} into account, we prepared two quite rigid cyclic chains, that is, cyclic amylose tris(phenylcarbamate) (cATPC, Chart 1)¹⁹ and cyclic amylose tris(*n*-butylcarbamate) (cATBC).²⁰ Their dimensional and hydrodynamic properties in ethers and alcohols were successfully explained by the current theories^{21,22} for the wormlike ring with substantially the same molecular parameters for the corresponding linear polymer. The chain stiffness ranges from 11 to 75 nm in the Kuhn segment length λ^{-1} (twice that of the persistence length) in terms of the wormlike chain.²³ This high chain stiffness is

Chart 1. Chemical Structures of Cyclic Amylose Tris(phenylcarbamate) (1, cATPC) and Solvents: Methyl Acetate (2, MEA), Ethyl Acetate (3, EA), and 4-Methyl-2-pentanone (4, MIBK)



mainly stabilized by the intramolecular hydrogen bonds of NH and C=O groups on neighboring units.^{18,24,25} Indeed, the chain stiffness of linear amylose carbamates is significantly higher than those for typical flexible chains, that is, 2 nm for polystyrene in cyclohexane²⁶ and 4 nm for amylose in dimethyl sulfoxide.²⁷ Furthermore, the positive second virial coefficient

Received: July 4, 2013

Revised: July 19, 2013

Published: July 23, 2013

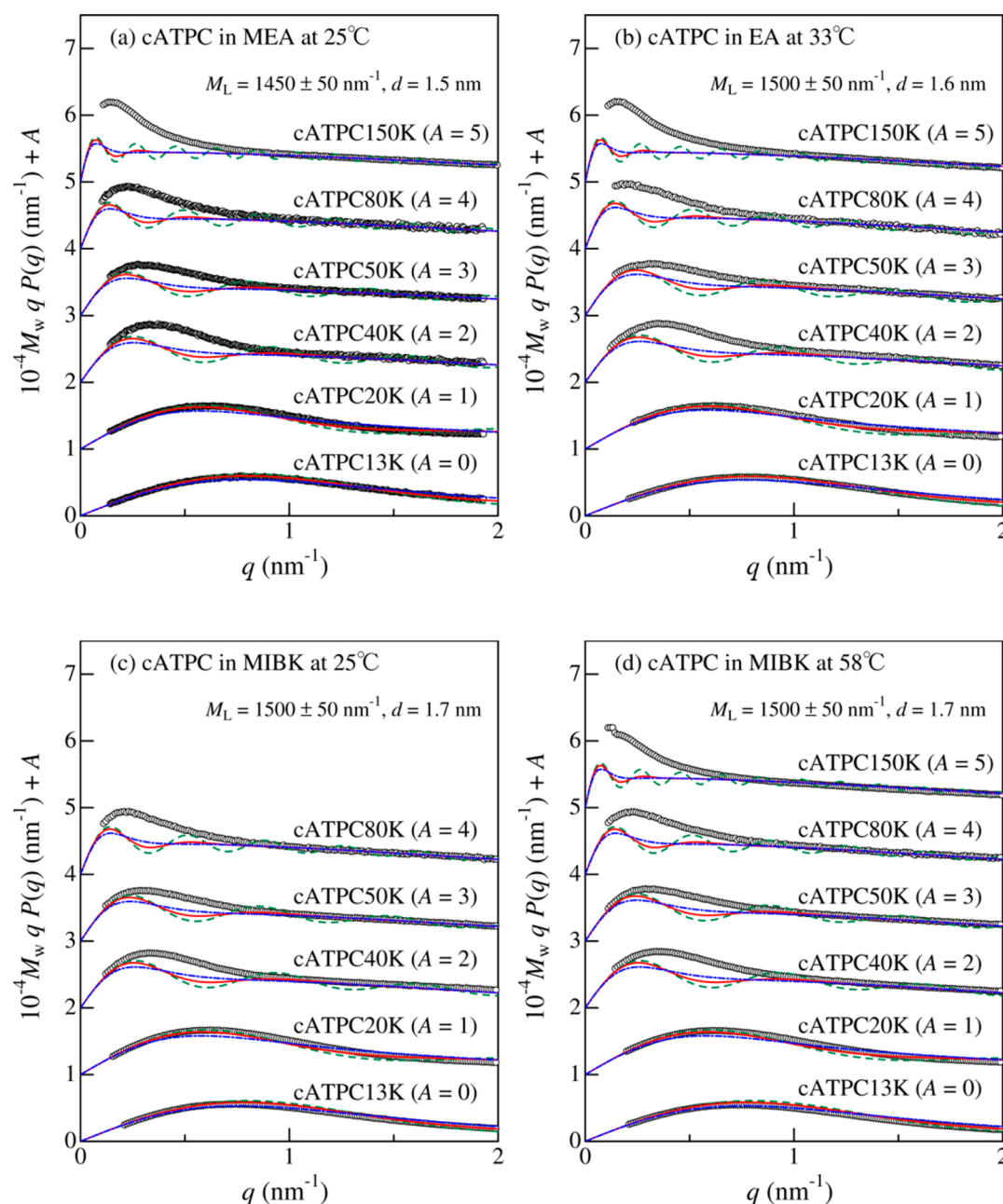


Figure 1. Reduced Holtzer plots for indicated cATPC samples in MEA at 25 °C (a), in EA at 33 °C (b), in MIBK at 25 °C (c), and in MIBK at 58 °C (d). Dashed (green), solid (red), and dot-dashed (blue) curves indicate theoretical values for cylindrical rigid rings with $M_w/M_n = 1, 1.05$, and 1.2 , respectively. See the text for theoretical details. The ordinate values are shifted by A for clarity.

A_2 were observed for cATBC in 2-propanol at the Θ temperature. The obtained A_2 values were also explained by a current simulation result for wormlike ring²⁸ which considers intermolecular topological interaction. This apparently repulsive intermolecular interaction is caused because the two discrete rings may not become linked rings without cutting at least one covalent bond of the main chain.^{29,30} Consequently, the above-mentioned specific behavior on rigid ring polymers was not seen in spite of the high stiffness, and therefore, the behavior might be found for some other ring polymers of which local conformation is more effectible by the environment.

We recently suggested that NH groups of linear amylose tris(phenylcarbamate) (ATPC) in ketones and esters form intermolecular hydrogen bonding with the C=O group of the solvent molecules. The main chains are appreciably extended

and stiffened because the NH groups of ATPC locate inside surrounded by the main chain and the other phenyl groups. This behavior is detectable as increases both of λ^{-1} and the helix pitch per residue h .^{31,32} Indeed, the effect becomes more significant with increasing the size of solvent molecules, that is, methyl acetate (MEA) < ethyl acetate (EA) < 4-methyl-2-pentanone (MIBK). Thus, we expected that the finite curvature of our cATPC samples may influence the hydrogen bonding behavior and hence the local helical structure and the chain stiffness would be different from those for linear ATPC.

To elucidate the dimensional behavior of cATPC chains in such solvents, small-angle X-ray scattering (SAXS) and static and dynamic light scattering measurements were carried out for cATPC samples in MEA, EA, and MIBK to compare their dimensional and hydrodynamic properties with those for the

linear polymer. Since the three solvents are the Θ solvent of linear ATPC of which Θ temperatures were estimated to be ~ 25 ,³¹ 33 ,³¹ and 58 °C (see Figure S5) in MEA, EA, and MIBK, respectively, A_2 was also determined around the Θ temperature to ascertain whether the difference in the local conformation affects the intermolecular interactions.

EXPERIMENTAL SECTION

Samples and Solvents. Six previously investigated cATPC samples¹⁹ ranging in molar mass from 1.3×10^4 to 1.5×10^5 were used for this study. These samples were prepared from enzymatically synthesized cyclic amylose in the manner reported previously^{13,33} and the weight-average molar mass M_w of each sample was determined. The degree of substitution (DS) and the dispersity index (DI) defined as the ratio of M_w to the number-average molar mass M_n were estimated to be 3.0 ± 0.2 and 1.13 ± 0.08 , respectively. Five linear ATPC samples, ATPC20K, ATPC50K, ATPC300K, ATPC500K, and ATPC800K, of which molecular characteristics (M_w , DS, and DI) were listed in ref 25, were also used in this study. One more linear ATPC sample ATPC3M-2 was further prepared from enzymatically synthesized linear amylose having quite narrow DI (~ 1.1) and no branching with the same methods reported previously.²⁵ The values of M_w and DS were determined to be 2.97×10^6 and 3.0 , respectively. The following four solvents MEA, EA, MIBK, and 1,4-dioxane (DIOX) were purified by fractional distillation over calcium hydride.

Small-Angle X-ray Scattering. Synchrotron radiation SAXS measurements were performed for all the cATPC samples in MEA at 25 °C, in EA at 33 °C, and in MIBK at 25 and 58 °C and for ATPC20K and ATPC50K in MIBK and DIOX both at 58 °C. Four solutions with different polymer mass concentration c for each sample were measured to determine the z -average mean-square radius of gyration $\langle S^2 \rangle_z$ and the particle scattering function $P(q)$. As X-ray sources, the BL40B2 beamline in SPring-8 (Hyogo, Japan) or the BL-10C beamline in KEK-PF (Ibaraki, Japan) were used in this study. The scattered light was detected by using a Rigaku R-Axis VII imaging plate detector. The wavelength was set to be 0.10 (SPring-8) and 0.15 nm (KEK-PF). The camera lengths used are 1500 or 4000 (SPring-8) or 2000 mm (KEK-PF). The magnitude of the scattering vector q at each pixel on the imaging plate was determined from the diffraction pattern of silver behenate. The scattering intensity at each q was determined from the circular average of the pixels having substantially the same q . The obtained scattering intensity $I(q)$ was analyzed in terms of the Guinier plot for cATPC samples and the Berry plot for linear ATPC samples to determine $P(q)$ and $\langle S^2 \rangle_z$ (see Figure S1 in the Supporting Information for the plots). See ref 20 for more details of experimental procedures and data analyses.

Static and Dynamic Light Scattering. Light scattering measurements were made for cATPC samples in the three solvents on an ALV/DLS/SLS-5000 light scattering photometer equipped with an ALV-500E/WIN photon correlator. Static light scattering measurements were carried out for the following samples, solvents, and temperatures: cATPC50K and cATPC80K in MEA at 25 °C, cATPC50K, cATPC80K, and cATPC150K in EA between 25 and 45 °C, and cATPC50K, cATPC80K, ATPC500K, and ATPC3M-2 in MIBK between 25 and 60 °C. Dynamic light scattering measurements were carried out for cATPC50K and cATPC80K in MEA at 25 °C,

in EA at 33 °C, and in MIBK at 58 °C, and cATPC150K in EA at 33 °C. The obtained data were analyzed by using the plots of $\ln[g^{(2)}(t) - 1]$ vs $q^2 t$ to determine the first cumulant Γ (Figure S2 in the Supporting Information), where $g^{(2)}(t)$ denotes the normalized autocorrelation function of scattering light intensity at time t . The hydrodynamic radius R_H was calculated by means of the Stokes–Einstein equation from the translational diffusion coefficient, which was determined by the extrapolation of Γ/q^2 to $c = 0$ and $q^2 = 0$.

RESULTS AND DISCUSSION

Chain Dimensions and Wormlike Chain Analysis. The Holtzer plots, $qP(q)$ vs q , are illustrated in Figure 1 for the cATPC samples in MEA at 25 °C, in EA at 33 °C, and in MIBK at 25 and 58 °C. The $P(q)$ data for each sample are essentially independent of the solvent and temperature investigated, suggesting that the local conformation does not depend significantly on the solvent. While theoretical formulation of $P(q)$ for the wormlike ring has not been reported yet, $P(q)$ for the rigid ring having cylindrical cross section (torus) can be written as¹⁹

$$P(q) = \int_0^{\pi/2} \left[4J_0\left(\frac{Lq \sin \xi}{2\pi}\right) J_1\left(\frac{dq}{2}\right) / dq \right]^2 \sin \xi \, d\xi \quad (1)$$

where, d is the diameter of the cylinder, $J_n(x)$ the Bessel function of the n th order, and L the contour length, which is related to the molar mass per unit contour length M_L as

$$L = M/M_L \quad (2)$$

Here, M denotes the molar mass of the torus. We recently showed that the theoretical $P(q)$ for the rigid ring reproduces the experimental data consistently except for the data at the lower q region for high molar mass samples, at which flexibility of the main chain may significantly affect the value of $P(q)$. If we assume log-normal distribution³⁴ and appropriate DI, that is, $M_w/M_n = 1.05$ and 1.2 , each $P(q)$ is mostly reproduced by the theoretical values except for low q range for four high M_w samples. It should be noted that the theoretical $P(q)$ for the monodisperse rigid ring cannot reproduce the experimental data since it fluctuates even at high q range (see the green dashed curves in Figure 1). The obtained parameters are $M_L = 1450 \pm 50 \text{ nm}^{-1} \text{ g mol}^{-1}$ and $d = 1.5$ nm in MEA at 25 °C, $M_L = 1500 \pm 50 \text{ nm}^{-1} \text{ g mol}^{-1}$ and $d = 1.6$ nm in EA at 33 °C, $M_L = 1500 \pm 50 \text{ nm}^{-1} \text{ g mol}^{-1}$ and $d = 1.7$ nm in MIBK at 25 °C, and $M_L = 1500 \pm 50 \text{ nm}^{-1} \text{ g mol}^{-1}$ and $d = 1.7$ nm in MIBK at 58 °C. The M_L value in MEA is quite close to that for linear ATPC ($1390 \pm 20 \text{ nm}^{-1} \text{ g mol}^{-1}$)³¹ as is the case with the previously investigated five systems.^{19,20} On the contrary, the value in MIBK is significantly larger than that for the linear one ($1230 \pm 40 \text{ nm}^{-1} \text{ g mol}^{-1}$)³¹, indicating that local helical structure of cATPC in MIBK should be appreciably different from that for the linear polymer.

Gyration radius $\langle S^2 \rangle_z$ data summarized in Table 1 are plotted against M_w in Figure 2 along with those for linear ATPC.^{25,31} While the ratio g_s of $\langle S^2 \rangle_z$ for the ring polymer to that for the linear one having the same molar mass is about 0.50 for cATPC in DIOX and the wormlike chain parameters for cATPC are substantially the same as those for the linear one, appreciably smaller g_s values are obtained for cATPC in MEA, EA, and MIBK, that is, 0.42 in MEA at 25 °C, 0.30 in EA at 33 °C, 0.35 in MIBK at 58 °C, and 0.25 in MIBK at 25 °C, suggesting that cATPC has significantly different wormlike chain parameters in

Table 1. Weight-Average Molar Mass M_w and z -Average Radius of Gyration $\langle S^2 \rangle_z^{1/2}$ for cATPC in MEA at 25 °C, in EA at 33 °C, and in MIBK at 58 and 25 °C

sample	$M_w/10^4$ (g mol ⁻¹) ^a	$\langle S^2 \rangle_z^{1/2}$ (nm)			
		in MEA at 25 °C	in EA at 33 °C	in MIBK at 58 °C	in MIBK at 25 °C
cATPC13K	1.25	1.58	1.58	1.67	1.65
cATPC20K	1.83	2.15	2.10	2.10	2.05
cATPC40K	4.46	4.0	3.9	4.0	4.1
cATPC50K	4.73	4.7	4.6	4.6	4.7
cATPC80K	8.19	6.8	6.4	6.7	6.8
cATPC150K	14.9	9.5	9.2	9.5	

^aReference 19.

EA and MIBK from that for linear ATPC in the corresponding solvent.

Theoretical radius of gyration $\langle S^2 \rangle_{0,l}$ and $\langle S^2 \rangle_{0,c}$ for linear and cyclic wormlike chains can be calculated by the Benoit–Doty³⁵

and the Shimada–Yamakawa²¹ equations (eq 3 for linear and eq 4 for ring):

$$\langle S^2 \rangle_{0,l} = \lambda^2 \left\{ \frac{\lambda L}{6} - \frac{1}{4} + \frac{1}{4\lambda L} - \frac{1}{8\lambda^2 L^2} [1 - \exp(-2\lambda L)] \right\} \quad (3)$$

$$\begin{aligned} \langle S^2 \rangle_{0,c} &= \frac{L^2}{4\pi^2} \left[1 - 0.1140\lambda L - 0.0055258(\lambda L)^2 \right. \\ &\quad \left. + 0.0022471(\lambda L)^3 - 0.00013155(\lambda L)^4 \right] \\ &\quad \text{for } \lambda L \leq 6 \\ &= \frac{L}{12\lambda} \left\{ 1 - \frac{7}{6\lambda L} - 0.025 \exp[-0.01(\lambda L)^2] \right\} \\ &\quad \text{for } \lambda L \geq 6 \end{aligned} \quad (4)$$

The radius of gyration $\langle S^2 \rangle$ for cylindrical wormlike rings may be written as

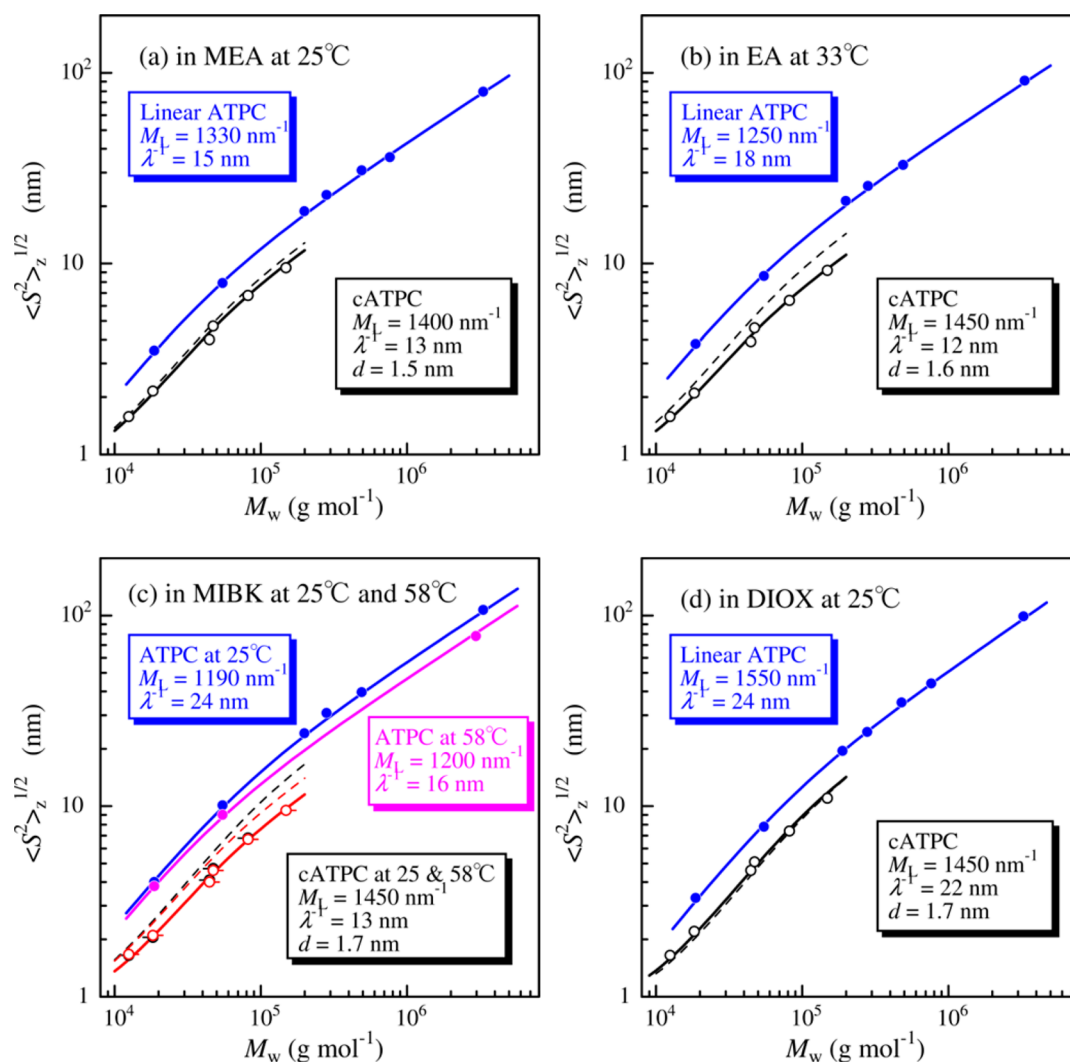


Figure 2. Molar mass dependence of $\langle S^2 \rangle_z^{1/2}$ for cATPC (unfilled circles) and linear ATPC (filled circles)^{25,31} in MEA at 25 °C (a), in EA at 33 °C (b), in MIBK at 58 and 25 °C (c), and in DIOX at 25 °C (d).¹⁹ In panel c, red and magenta symbols indicate the data points at 58 °C. Solid black (or red) and blue (or magenta) curves indicate theoretical curves for cylindrical wormlike ring and linear chains, respectively, calculated with the parameters listed in each figure; those for linear ATPC in DIOX and MIBK at 25 °C include intramolecular excluded volume effects (see refs 22 and 24 for details). Dashed lines are theoretical values for the wormlike ring with the parameters for linear ATPC.

$$\langle S^2 \rangle = \langle S^2 \rangle_{0,c} + \frac{d^2}{4} \quad (5)$$

since $\langle S^2 \rangle$ for a cylindrical rigid ring is expressed as

$$\langle S^2 \rangle = \frac{L^2}{4\pi^2} + \frac{d^2}{4} \quad (6)$$

It should be noted that the chain thickness effect was negligible for linear ATPC samples^{25,31} because of higher $\langle S^2 \rangle_z$ for linear ATPC even for the lowest M_w sample. The theoretical $g_s \equiv \langle S^2 \rangle / \langle S^2 \rangle_{0,l}$ value at $M = 10^5$ was calculated with the parameters for ATPC in investigated solvents to be ~ 0.5 , which is close to that in DIOX but slightly or significantly larger than those in the other solvents. Indeed, dashed curves calculated for $\langle S^2 \rangle^{1/2}$ with M_L and λ^{-1} for linear ATPC^{22,24} and d determined from $P(q)$ for cATPC significantly overestimate the experimental data in EA and MIBK as shown in Figure 2. Assuming the d value from $P(q)$, the other two parameters, M_L and λ^{-1} , can be determined from a curve-fitting procedure to be $M_L = 1400 \text{ nm}^{-1} \text{ g mol}^{-1}$ and $\lambda^{-1} = 13 \text{ nm}$ in MEA, $M_L = 1450 \text{ nm}^{-1} \text{ g mol}^{-1}$ and $\lambda^{-1} = 12 \text{ nm}$ in EA, and $M_L = 1450 \text{ nm}^{-1} \text{ g mol}^{-1}$ and $\lambda^{-1} = 13 \text{ nm}$ in MIBK, in which the determination errors are $\pm 50 \text{ nm}^{-1} \text{ g mol}^{-1}$ for M_L and $\pm 2 \text{ nm}$ for λ^{-1} . The obtained M_L values are substantially the same as those determined from $P(q)$ in Figure 1 in the corresponding solvent.

Hydrodynamic radius R_H for cATPC in MEA at 25 °C, in EA at 33 °C, and in MIBK at 58 °C is plotted against M_w/M_0 in Figure 3 along with those for cATBC in 2-propanol at 35 °C²⁰

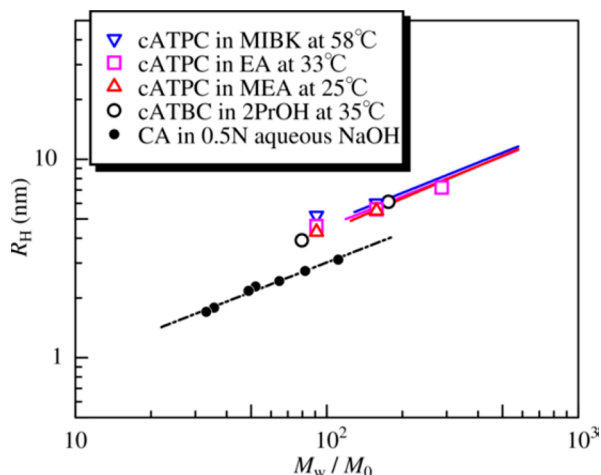


Figure 3. Plots of hydrodynamic radius R_H vs M_w/M_0 for cATPC in MEA at 25 °C (triangles), in EA at 33 °C (squares), in MIBK at 58 °C (inverted triangles) along with those for cATBC²⁰ in 2-propanol at 35 °C (unfilled circles) and cyclic amylose (CA) in 0.5 M aqueous NaOH (filled circles) at 25 °C.¹³ Solid curves are the theoretical values for the cylindrical wormlike ring (see text for the parameters).

and for cycloamylose (CA) in 0.5 M aqueous NaOH at 25 °C¹³ where M_0 denotes molar mass of the repeat unit, that is, $519.50 \text{ g mol}^{-1}$ for ATPC. The current data for cATPC are mostly the same as those for cATBC but significantly larger than those for CA. This is reasonable because λ^{-1} for cATPC is much larger than that for CA ($\sim 4 \text{ nm}$) and rather close to that for cATBC (20 nm) in 2-propanol. Fujii and Yamakawa²² formulated the translational friction coefficient for wormlike rings and the theoretical R_H can be calculated with L , λ^{-1} , and d . The last parameter d from hydrodynamic properties is usually different

from those for dimensional properties³⁶ including ATPC.^{25,31,32} Colored lines in the figure indicate the theoretical values with $d = 2.3, 3.1$, and 3.5 nm in MEA, EA, and MIBK, respectively with M_L and λ^{-1} determined from $P(q)$ and $\langle S^2 \rangle_z$. While the left end is the limitation of the theory, each line fit the experimental data for higher M_w samples almost quantitatively. Thus, the wormlike ring model is suitable to reproduce the experimental R_H of cATPC in the three solvents. However, it should be noted that R_H changes sensitively by d , and therefore a small difference in M_L and λ^{-1} cannot be recognized only from R_H . Indeed, data points for cATPC in DIOX (not shown here) of which λ^{-1} is 22 nm are substantially the same as those in the other solvents.

In our previous study for linear ATPC, we did not obtain solution properties at 58 °C. Thus, wormlike chain parameters for linear ATPC in MIBK and DIOX at 58 °C were also determined in the manner reported in our previous papers^{25,31} from $\langle S^2 \rangle_z$ in Figure 2, $P(q)$, and the intrinsic viscosity $[\eta]$ (see Figures S3 and S4 in the Supporting Information for the Holtzer plots and M_w dependence of $[\eta]$, respectively). For MIBK solutions, the following theories for cylindrical wormlike chains were used to analyze the solution data, that is, the Nakamura–Norisuye theory³⁷ for $P(q)$, the Benoit–Doty equation (eq 3)³⁵ for $\langle S^2 \rangle_z$, and the Yamakawa–Fujii–Yoshizaki theory^{38,39} for $[\eta]$. The M_L and λ^{-1} obtained from the different methods are consistent with each other. On the other hand, the $[\eta]$ data in DIOX at 58 °C are excellently fitted by those at 25 °C and the wormlike chain parameters previously obtained at 25 °C successfully explain the $P(q)$ data at 58 °C, thus we concluded that M_L and λ^{-1} in DIOX at 58 °C are essentially the same as those at 25 °C.

Molecular Characteristics. Table 2 summarizes the obtained wormlike chain parameters along with those for

Table 2. Values of the Helix Pitch per Residue h , the Kuhn Segment Length λ^{-1} , and the Chain Diameter d for cATPC and ATPC in MEA, MIBK, DIOX, and 2-Ethoxyethanol (2EE) at 25 °C, in EA at 33 °C, and in MIBK at 58 °C

solvent	temp (°C)	cATPC		ATPC	
		h (nm)	λ^{-1} (nm)	h (nm)	λ^{-1} (nm)
MEA	25	0.36 ± 0.02	13 ± 2	0.37 ± 0.02^a	15 ± 2^a
EA	33	0.35 ± 0.02	12 ± 2	0.39 ± 0.01^a	17 ± 2^a
MIBK	58	0.35 ± 0.02	13 ± 2	0.42 ± 0.02	17 ± 2
MIBK	25	0.35 ± 0.02	13 ± 2	0.42 ± 0.02^a	24 ± 2^a
DIOX	25 and 58 ^d	0.34 ± 0.02^c	22 ± 3^c	0.34 ± 0.01^b	22 ± 2^b
2EE	25	0.32 ± 0.02^c	16 ± 3^c	0.32 ± 0.01^b	16 ± 2^b

^aReference 31. ^bReference 25. ^cReference 19. ^dOnly for ATPC.

linear ATPC,^{25,31} that is, λ^{-1} and the helix pitch per residue h , which is related to M_L by $h = M_0/M_L$. As depicted in our previous paper, both λ^{-1} and h for linear ATPC increase with increasing molar volume v_M of the solvent; the values are determined from the density to be $79.9 \text{ cm}^3 \text{ mol}^{-1}$ for MEA at 25 °C, $99.6 \text{ cm}^3 \text{ mol}^{-1}$ for EA at 33 °C, 125.8 and $130.9 \text{ cm}^3 \text{ mol}^{-1}$ for MIBK at 25 and 58 °C, respectively. Thus, both h and λ^{-1} are plotted against v_M in Figure 4. While these parameters for linear ATPC monotonically increase with increasing v_M except for λ^{-1} at 58 °C, those for cATPC are independent of the solvent. In other words, we first demonstrate that rigid ring polymers may have different local

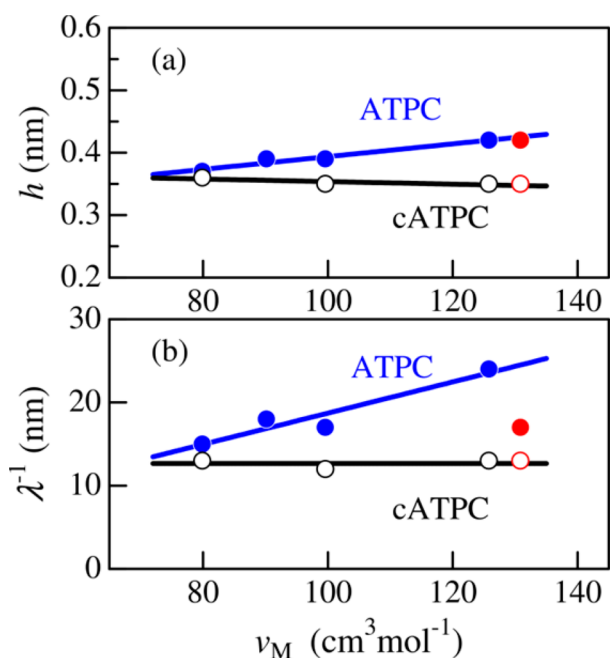


Figure 4. Dependences of h (a) and λ^{-1} (b) on ν_M for cATPC (black unfilled circles at 25 or 33 °C, red unfilled circles at 58 °C) and ATPC in ketones and esters (blue filled circles at 25 or 33 °C, red filled circles at 58 °C).

conformation from that for the corresponding linear chain. But, we note that this effect is not seen for every rigid ring. In actuality, dimensional properties of previously studied five rigid cyclic polymer–solvent systems of which λ^{-1} ranges between 11 and 75 nm are well explained by the wormlike ring model having essentially the same molecular parameters as the corresponding linear polymer–solvent system. Considering that the significant ν_M dependence of h and λ^{-1} for linear ATPC is due to the size of hydrogen bonding solvent molecules, the number of such solvent molecules for cATPC may be fewer than the linear one and it is not enough to extend and to stiffen the cATPC main chain. Since linear ATPC and similar derivatives⁴⁰ are useful as the chiral stationary phase, the above result indicates that cATPC may have different interaction with chiral small molecules from that for the linear one. Of course, it should be expected that dimensional properties for cATPC with much higher molar mass samples should be described by the wormlike chain parameters for the linear chain in the corresponding solvent. The molar mass of the current cATPC samples should be too small to observe the molar mass dependent conformational change. Regarding this, λ^{-1} for linear ATPC in MIBK at 58 °C is significantly smaller than that at 25 °C as shown in Table 2 whereas the same value of 22 nm was obtained in DIOX at both 25 and 58 °C, indicating that high chain stiffness stabilized by hydrogen bonding MIBK molecules is easily effectible by raising temperature while the chain stiffness stabilized by the intramolecular hydrogen bond (ATPC in DIOX) is more stable against the temperature change.

Intermolecular Interactions. Figure 5 shows the temperature dependence of the second virial coefficient A_2 for ATPC in EA and MIBK. Data points for cATPC decrease with raising temperature as is the case with linear ATPC. We did not show the A_2 data in MEA since those for linear ATPC vanish at 25 °C but the temperature dependence is too small to estimate the

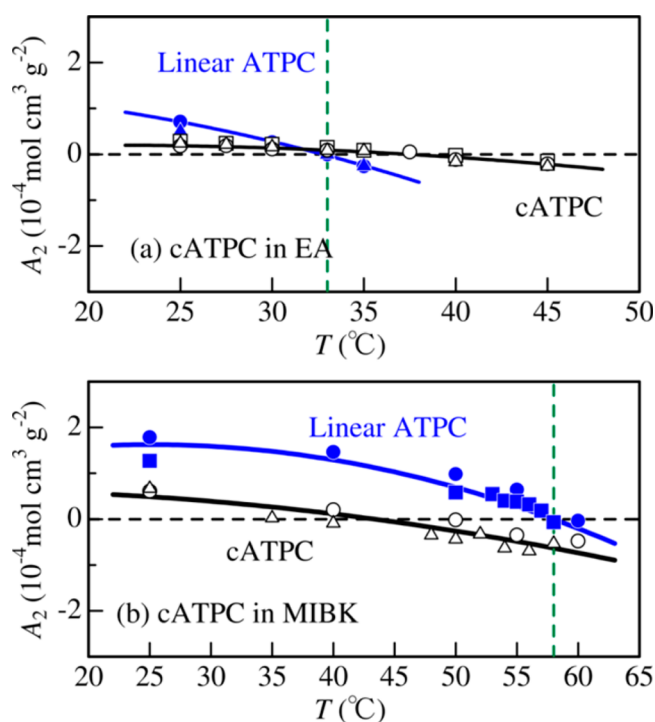


Figure 5. Temperature dependence of the second virial coefficients A_2 for cATPC50K (unfilled circles), cATPC80K (unfilled triangles), and cATPC150K (unfilled squares) in EA (a) and MIBK (b), along with A_2 for linear ATPC samples, ATPC500K ($M_w = 4.91 \times 10^5$, filled circles), ATPC3M ($M_w = 3.33 \times 10^6$, filled triangles), and ATPC3M-2 ($M_w = 2.97 \times 10^6$, filled squares).

Θ temperature.³¹ The A_2 values for cATPC at the Θ temperature for linear ATPC (at 25 °C for MEA solution) are summarized in Table 3. While cATBC has a large positive

Table 3. Second Virial Coefficient A_2 for cATPC in MEA at 25 °C, in EA at 33 °C, and in MIBK at 58 °C

sample	A_2 (10^{-4} mol g $^{-2}$ cm 3)		
	in MEA at 25 °C	in EA at 33 °C	in MIBK at 58 °C
cATPC50K	0.33	0.09	−0.43 ^a
cATPC80K	0.73	0.09	−0.53
cATPC150K		0.15	

^aEstimated by interpolation of the data at 55 and 60 °C.

A_2 of $\sim 1.4 \times 10^{-4}$ mol cm 3 g $^{-2}$ in 2-propanol at the Θ temperature, smaller (but still positive) values are obtained in MEA, they mostly vanish in EA, and furthermore, the values are negative in MIBK. This may be unreasonable because interaction between ring polymers should be repulsive even in Θ solvent.^{29,30} According to Ida et al.,²⁸ A_2 for reduced second virial coefficient $A_2 M_L^2 / 4 \lambda^{-1} N_A$ for the wormlike ring is found from the simulation method to be a function of λL , where N_A denotes the Avogadro number. Their values fitted well our recent data for cATBC in 2-propanol²⁰ and fairly explained those for the more flexible ring polymer, cyclic polystyrene, of which λ^{-1} is about 2 nm.²⁶ We thus compare the simulation result with the experimental values in Figure 6 in which the data points for cATBC in 2-propanol²⁰ and cyclic polystyrene in cyclohexane.^{3,8,9} The discrepancy between experimental and simulation result for cATPC becomes larger with increasing ν_M , that is in the order of MEA, EA, and MIBK.

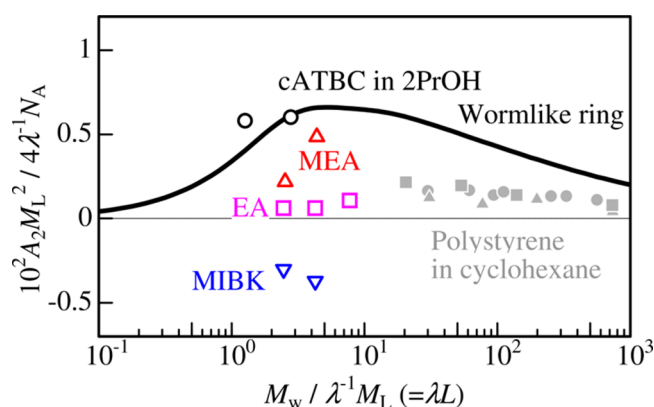


Figure 6. Reduced chain length ($\lambda L = M_w / \lambda^{-1} M_L$) dependence of reduced second virial coefficient ($A_2 M_L^2 / 4 \lambda^{-1} N_A$) for cATPC in MEA (unfilled triangles), EA (unfilled squares), and MIBK (inverted triangles) at the corresponding Θ temperatures along with those for cATBC in 2-propanol (unfilled circles) at the Θ temperature (35 °C) and for cyclic polystyrene in cyclohexane (filled circles, Roovers et al.;³ filled triangles, Huang et al.;⁸ filled squares, Takano et al.⁹) at the Θ temperature (34.5–35 °C). Solid curve are results from Monte Carlo simulation by Ida et al.²⁸

This is most likely because the monomeric unit having the shrunk helical structure becomes more attractive with the monomeric site of the other cATPC chain. This effect is still smaller for MEA solution than the intermolecular topological interaction and becomes mostly equivalent in EA, and furthermore, it is much larger than the topological interaction in MIBK. Thus, we may conclude that rather stiff cyclic polymers may change not only the chain dimensions but also intermolecular interactions.

CONCLUSIONS

The helix pitch per residue and the chain stiffness of cyclic ATPC in ketones and esters are independent of the solvent whereas both of them for linear ATPC appreciably increase with increasing the size of solvent molecule, indicating that the local helical structure and the chain stiffness of rather rigid rings may not be the same as those for the corresponding linear polymer if the polymer chains have finite chain stiffness. This conformational difference is likely due to the different solvation structure. Consequently, the intermolecular interaction between monomeric units of two different cATPC chains estimated in such solvents is significantly different from that for linear ATPC in the corresponding solvent.

ASSOCIATED CONTENT

Supporting Information

Guinier plots for cATPC samples, raw dynamic light scattering data, the Holtzer plots for linear ATPC in DIOX and MIBK at 58 °C, and molar mass dependence of the intrinsic viscosity for linear ATPC in DIOX and MIBK at 25 and 58 °C. This material is available free of charge via the Internet at <http://pubs.acs.org>.

AUTHOR INFORMATION

Corresponding Author

*E-mail: kterao@chem.sci.osaka-u.ac.jp.

Notes

The authors declare no competing financial interest.

ACKNOWLEDGMENTS

The synchrotron radiation experiments were performed at the BL40B2 in SPring-8 with the approval of the Japan Synchrotron Radiation Research Institute (JASRI) (Proposal Nos. 2010B1126, 2011A1049, and 2011B1068) and at the BL-10C in KEK-PF under the approval of the Photon Factory Program Advisory Committee (No. 2010G080). We thank Professor Takahiro Sato (Osaka University) for fruitful discussion. This work was partially supported by JSPS KAKENHI Grant No. 23750128.

REFERENCES

- (1) Dodgson, K.; Sympton, D.; Semlyen, J. A. Studies of Cyclic and Linear Poly(dimethyl siloxanes): 2. Preparative Gel-Permeation Chromatography. *Polymer* **1978**, *19*, 1285–1289.
- (2) Higgins, J. S.; Dodgson, K.; Semlyen, J. A. Studies of Cyclic and Linear Poly(dimethyl siloxanes). 3. Neutron-Scattering Measurements of the Dimensions of Ring and Chain Polymers. *Polymer* **1979**, *20*, 553–558.
- (3) Roovers, J.; Toporowski, P. M. Synthesis of High Molecular-Weight Ring Polystyrenes. *Macromolecules* **1983**, *16*, 843–849.
- (4) Ragnetti, M.; Geiser, D.; Hocker, H.; Oberthur, R. C. Small-Angle Neutron-Scattering (SANS) of Cyclic and Linear Polystyrene in Toluene. *Makromol. Chem., Macromol. Chem. Phys.* **1985**, *186*, 1701–1709.
- (5) Lutz, P.; McKenna, G. B.; Rempp, P.; Strazielle, C. Solution Properties of Ring-Shaped Polystyrenes. *Makromol. Chem. Rapid Commun.* **1986**, *7*, 599–605.
- (6) Hadziioannou, G.; Cotts, P. M.; Tenbrinke, G.; Han, C. C.; Lutz, P.; Strazielle, C.; Rempp, P.; Kovacs, A. J. Thermodynamic and Hydrodynamic Properties of Dilute-Solutions of Cyclic and Linear Polystyrenes. *Macromolecules* **1987**, *20*, 493–497.
- (7) McKenna, G. B.; Hostetter, B. J.; Hadjichristidis, N.; Fetters, L. J.; Plazek, D. J. A Study of the Linear Viscoelastic Properties of Cyclic Polystyrenes Using Creep and Recovery Measurements. *Macromolecules* **1989**, *22*, 1834–1852.
- (8) Huang, J. X.; Shen, J.; Li, C. R.; Liu, D. Z. A New Theoretical Approach to Problems of the Solution Behavior of Ring-Shaped Polymers. *Makromol. Chem., Macromol. Chem. Phys.* **1991**, *192*, 1249–1254.
- (9) Takano, A.; Kushida, Y.; Ohta, Y.; Masuoka, K.; Matsushita, Y. The Second Virial Coefficients of Highly-Purified Ring Polystyrenes in Cyclohexane. *Polymer* **2009**, *50*, 1300–1303.
- (10) Takano, A.; Ohta, Y.; Masuoka, K.; Matsubara, K.; Nakano, T.; Hieno, A.; Itakura, M.; Takahashi, K.; Kinugasa, S.; Kawaguchi, D.; Takahashi, Y.; Matsushita, Y. Radii of Gyration of Ring-Shaped Polystyrenes with High Purity in Dilute Solutions. *Macromolecules* **2012**, *45*, 369–373.
- (11) Kitamura, S.; Isuda, H.; Shimada, J.; Takada, T.; Takaha, T.; Okada, S.; Mimura, M.; Kajiwara, K. Conformation of Cyclo-maltooligosaccharide ("Cycloamylose") of dp21 in Aqueous Solution. *Carbohydr. Res.* **1997**, *304*, 303–314.
- (12) Shimada, J.; Kaneko, H.; Takada, T.; Kitamura, S.; Kajiwara, K. Conformation of Amylose in Aqueous Solution: Small-Angle X-ray Scattering Measurements and Simulations. *J. Phys. Chem. B* **2000**, *104*, 2136–2147.
- (13) Nakata, Y.; Amitani, K.; Norisuye, T.; Kitamura, S. Translational Diffusion Coefficient of Cycloamylose in Aqueous Sodium Hydroxide. *Biopolymers* **2003**, *69*, 508–516.
- (14) Schappacher, M.; Deffieux, A. Synthesis of Macrocyclic Copolymer Brushes and Their Self-Assembly into Supramolecular Tubes. *Science* **2008**, *319*, 1512–1515.
- (15) Lahasky, S. H.; Serem, W. K.; Guo, L.; Garno, J. C.; Zhang, D. H. Synthesis and Characterization of Cyclic Brush-Like Polymers by *N*-Heterocyclic Carbene-Mediated Zwitterionic Polymerization of *N*-Propargyl *N*-Carboxyanhydride and the Grafting-to Approach. *Macromolecules* **2011**, *44*, 9063–9074.

- (16) Zhang, K.; Tew, G. N. Cyclic Brush Polymers by Combining Ring-Expansion Metathesis Polymerization and the "Grafting from" Technique. *ACS Macro Lett.* **2012**, *1*, 574–579.
- (17) Burchard, W. In *Soft-Matter Characterization*; Borsali, R., Pecora, R., Eds.; Springer: Berlin, Germany, 2008; Vol. 1, pp 465–603.
- (18) Terao, K.; Murashima, M.; Sano, Y.; Arakawa, S.; Kitamura, S.; Norisuye, T. Conformational, Dimensional, and Hydrodynamic Properties of Amylose Tris(*n*-butylcarbamate) in Tetrahydrofuran, Methanol, and Their Mixtures. *Macromolecules* **2010**, *43*, 1061–1068.
- (19) Terao, K.; Asano, N.; Kitamura, S.; Sato, T. Rigid Cyclic Polymer in Solution: Cycloamylose Tris(phenylcarbamate) in 1,4-Dioxane and 2-Ethoxyethanol. *ACS Macro Lett.* **2012**, *1*, 1291–1294.
- (20) Terao, K.; Shigeuchi, K.; Oyamada, K.; Kitamura, S.; Sato, T. Solution Properties of a Cyclic Chain Having Tunable Chain Stiffness: Cyclic Amylose Tris(*n*-butylcarbamate) in Θ and Good Solvents. *Macromolecules* **2013**, *46*, 5355–5362.
- (21) Shimada, J.; Yamakawa, H. Moments for DNA Topoisomers: The Helical Wormlike Chain. *Biopolymers* **1988**, *27*, 657–73.
- (22) Fujii, M.; Yamakawa, H. Moments and Transport Coefficients of Wormlike Rings. *Macromolecules* **1975**, *8*, 792–799.
- (23) Kratky, O.; Porod, G. Röntgenuntersuchung Geloster Fadenmoleküle. *Recl. Trav. Chim. Pays-Bas* **1949**, *68*, 1106–1122.
- (24) Bittiger, H.; Keilich, G. Optical Rotatory Dispersion and Circular Dichroism of Carbanilyl Polysaccharides. *Biopolymers* **1969**, *7*, 539–556.
- (25) Terao, K.; Fujii, T.; Tsuda, M.; Kitamura, S.; Norisuye, T. Solution Properties of Amylose Tris(phenylcarbamate): Local Conformation and Chain Stiffness in 1,4-Dioxane and 2-Ethoxyethanol. *Polym. J.* **2009**, *41*, 201–207.
- (26) Norisuye, T.; Fujita, H. Excluded-Volume Effects in Dilute Polymer Solutions. XIII. Effects of Chain Stiffness. *Polym. J.* **1982**, *14*, 143–147.
- (27) Nakanishi, Y.; Norisuye, T.; Teramoto, A.; Kitamura, S. Conformation of Amylose in Dimethyl-Sulfoxide. *Macromolecules* **1993**, *26*, 4220–4225.
- (28) Ida, D.; Nakatomi, D.; Yoshizaki, T. A Monte Carlo Study of the Second Virial Coefficient of Semiflexible Ring Polymers. *Polym. J.* **2010**, *42*, 735–744.
- (29) Edwards, S. F. Statistical Mechanics with Topological Constraints: I. *Proc. Phys. Soc., London* **1967**, *91*, 513–519.
- (30) Edwards, S. F. Statistical Mechanics with Topological Constraints: II. *J. Phys. A: Gen. Phys.* **1968**, *1*, 15–28.
- (31) Fujii, T.; Terao, K.; Tsuda, M.; Kitamura, S.; Norisuye, T. Solvent-Dependent Conformation of Amylose Tris(phenylcarbamate) as Deduced from Scattering and Viscosity Data. *Biopolymers* **2009**, *91*, 729–736.
- (32) Tsuda, M.; Terao, K.; Nakamura, Y.; Kita, Y.; Kitamura, S.; Sato, T. Solution Properties of Amylose Tris(3,5-dimethylphenylcarbamate) and Amylose Tris(phenylcarbamate): Side Group and Solvent Dependent Chain Stiffness in Methyl Acetate, 2-Butanone, and 4-Methyl-2-pentanone. *Macromolecules* **2010**, *43*, 5779–5784.
- (33) Takaha, T.; Yanase, M.; Takata, H.; Okada, S.; Smith, S. M. Potato D-Enzyme Catalyzes the Cyclization of Amylose to Produce Cycloamylose, a Novel Cyclic Glucan. *J. Biol. Chem.* **1996**, *271*, 2902–2908.
- (34) Practically, the theoretical $P(q)$ is not caused significantly by the distribution function and indeed $P(q)$ calculated by using Schultz–Zimm distribution is substantially close to the same as that for log-normal distribution.
- (35) Benoit, H.; Doty, P. Light Scattering from Non-Gaussian Chains. *J. Phys. Chem.* **1953**, *57*, 958–963.
- (36) Yamakawa, H. *Helical Wormlike Chains in Polymer Solutions*; Springer: Berlin, Germany, 1997.
- (37) Nakamura, Y.; Norisuye, T. Scattering Function for Wormlike Chains with Finite Thickness. *J. Polym. Sci., Part. B: Polym. Phys.* **2004**, *42*, 1398–1407.
- (38) Yamakawa, H.; Fujii, M. Intrinsic Viscosity of Wormlike Chains. Determination of the Shift Factor. *Macromolecules* **1974**, *7*, 128–135.
- (39) Yamakawa, H.; Yoshizaki, T. Transport Coefficients of Helical Wormlike Chains. 3. Intrinsic Viscosity. *Macromolecules* **1980**, *13*, 633–643.
- (40) Ikai, T.; Okamoto, Y. Structure Control of Polysaccharide Derivatives for Efficient Separation of Enantiomers by Chromatography. *Chem. Rev.* **2009**, *109*, 6077–6101.